Production and anisotropic flow of thermal photons in collisions of α-clustered carbon with heavy nuclei at relativistic energies

Pingal Dasgupta,[1,2] Rupa Chatterjee,[3,4,*] and Guo-Liang Ma (马国亮) [1,2,†]

[1]*Key Laboratory of Nuclear Physics and Ion-beam Application (MOE), Institute of Modern Physics, Fudan University, Shanghai 200433, China*
[2]*Shanghai Research Center for Theoretical Nuclear Physics, NSFC and Fudan University, Shanghai 200438, China*
[3]*Variable Energy Cyclotron Centre, 1/AF, Bidhan Nagar, Kolkata-700064, India*
[4]*Homi Bhabha National Institute, Training School Complex, Anushaktinagar, Mumbai 400094, India*

The presence of α-clustered structure in the light nuclei produces different exotic shapes in nuclear structure studies at low energies. Recent phenomenological studies suggest that collision of heavy nuclei with α-clustered carbon (^{12}C) at relativistic energies can lead to large initial state anisotropies. This is expected to impact the final momentum anisotropies of the produced particles significantly. The emission of electromagnetic radiations is considered to be more sensitive to the initial state compared to hadronic observables and thus photon observables are expected to be affected by the initial clustered structure profoundly. In this work we estimate the production and anisotropic flow of photons from most-central collisions of triangular α-clustered carbon and gold at $\sqrt{s_{NN}} = 200$ GeV using an event-by-event hydrodynamic framework and compare the results with those obtained from unclustered carbon and gold collisions. We show that the thermal photon v_3 for most central collisions is significantly large for the clustered case compared to the case with unclustered carbon, whereas the elliptic flow parameter does not show much difference for the two cases. In addition, the ratio of anisotropic flow coefficients is found to be a potential observable to constrain the initial state produced in relativistic heavy-ion collisions and also to know more about the α-clustered structure in carbon nucleus.

I. INTRODUCTION

Direct photons are considered as one of the cleanest probes to study the initial state and the evolution of the hot and dense matter produced in relativistic heavy-ion collisions. Various properties of the direct photon spectra and anisotropic flow parameters have been explored in detail in past two decades [1–10]. The most salient feature of the photon observables is their strong sensitivity to the initial conditions. Different collision geometries, initial-state fluctuations, the inclusion of initial state nucleon shadowing as well as slight variation of initial parameters in the model calculation have been found to affect the anisotropic flow parameters of photons significantly [11–17]. Thus, the study of direct photons from relativistic nuclear collisions offers an excellent opportunity to explore the hot and dense initial stage of quark-gluon plasma (QGP) produced in those collisions. However, it is important to mention that the inconsistency between the experimental photon anisotropic flow data and the results from theory calculations has been a subject of research for quite some time [18,19]. Realistic corrections in the initial conditions, upgraded hydrodynamical framework, and modified rates of thermal photon

production have been found to improve the theoretical calculation significantly [20–24].

In recent times, it has been shown that a large anisotropic flow of charged hadrons can appear even in small collision systems such as $p + p$, $p + A$, $d + A$, He $+ A$, etc. [25–27]. Significant initial-state anisotropies play a pivotal role in building up large final-state anisotropies for small systems. Recent interesting studies have suggested that the geometric effects of α clustering in the light nuclei (^{7,9}Be, ^{12}C, ^{16}O, etc.) can also be realized in the realm of relativistic nuclear collisions [28–32]. Similar attempts to identify nuclear deformations in heavy nuclei can be found in several studies [33–38].

Clustering has long been known to play a key role in understanding the structure of light nuclei. Over the past half-century, complex clusters of light nuclei have been discovered, especially for the typical 3α-clustered and 4α-clustered structures in ^{12}C and ^{16}O [39–44]. Many theories, such as antisymmetrized molecular dynamics (AMD) [45], fermionic molecular dynamics (FMD) [46], Tohsaki-Horiuchi-Schuck-Röpke (THSR) [47,48], and effective field-theory lattice calculations [49] attempt to explore possible geometries and even nonrigid structures of light nuclei. At present, the theoretical elucidation of the α structure in ^{12}C and ^{16}O is still a hard problem. Therefore, it is desirable to study the problem with some experimental probes [50–54]. Thus, experiments incorporating carbon and oxygen at the relativistic colliders

---
[*]rupa@vecc.gov.in
[†]glma@fudan.edu.cn

can be useful to shed light on the clustered structures. Studies based on kinetic theory and hydrodynamic model simulations have shown definitive and significant effects of α clustering on the anisotropic flow of hadrons at different collision energies lately [28–32]. The effect of α clustering on the direct photon signals in C + Au collisions at 200A GeV was first studied in Ref. [17]. It has been shown that specific orientations of the α-clustered C + Au collisions give rise to larger triangular flow (v_3) or elliptic flow (v_2) parameters considering a smooth initial energy density distribution [17]. In this work, we use a more realistic hydrodynamic framework to study the effect of clustered structure on different photon anisotropic flow (v_1, v_2, and v_3) observables in the most-central collision scenario. We expect that the properties emerging from this study will be useful for understanding the behavior of photon anisotropic flow parameters from similar colliding systems with α-clustered carbon at different beam energies.

The paper is organized as follows. In the next section, we briefly discuss the initial parameters and the framework for the model calculation. In Sec. III, we discuss the results of thermal photon spectra and anisotropic flow coefficients, and finally, we summarize the results in Sec. IV.

II. FRAMEWORK

In this study, we adapt a similar procedure used in Refs. [17,29] to prepare the initial conditions for α-clustered C + Au collisions at 200A GeV (see Appendix A). The initial conditions are subsequently evolved with a $(2+1)$-dimensional longitudinally boost invariant ideal relativistic hydrodynamic framework [55] to obtain the space-time evolution at midrapidity. The value of initial thermalization time is taken as $\tau_0 = 0.17$ fm/c and the transverse components of initial flow velocities (i.e., v_x and v_y) are neglected. A lattice-based equation of state (L&S) [56] is used in the hydrodynamic model and the constant freeze-out temperature (T_f) is taken as 160 MeV.

The thermal photon production from individual events is estimated by integrating the emission rates (i.e., $R = E\frac{dN}{d^3pd^4x}$) over the entire space-time evolution

$$E\frac{dN}{d^3p} = \int R(E^*(x), T(x))d^4x. \tag{1}$$

The $T(x)$ in the above equation is the local temperature and $E^*(x) = p^\mu u_\mu(x)$, where p^μ represents the four-momentum of photon and u_μ is the local four-velocity of the flow field. We use the complete next-to-leading order emission rates from Refs. [57,58] to evaluate photon production from the quark gluon plasma (QGP) phase and the parametrized rates from Ref. [59] for the hadronic sector.

The differential anisotropic flow coefficients [$v_n(p_T)$] and initial-state eccentricities are evaluated using the equations shown in Appendix A.

III. PRODUCTION AND ANISOTROPIC FLOW OF THERMAL PHOTONS

In the present study, we focus on the most central collisions where more geometry-dominated effects are expected to be seen. At present we do not have any knowledge about the
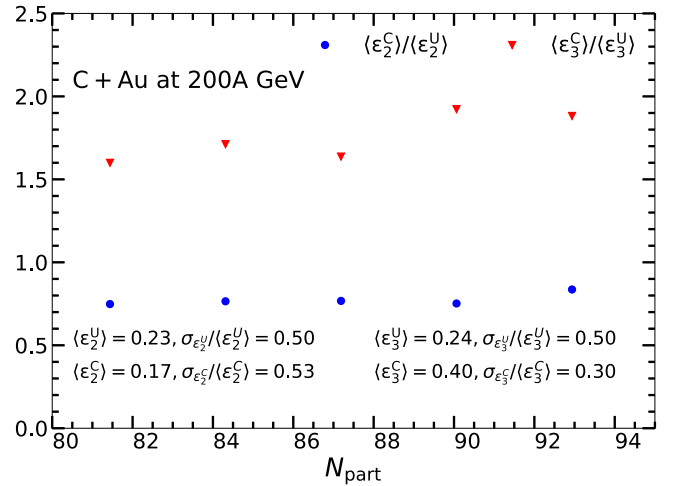

FIG. 1. The ratio of α-clustered to unclustered event-averaged initial state elliptic and triangular eccentricities as a function of N_{part} from C + Au collisions at 200A GeV.

minimum bias event distribution of charged hadrons from hydrodynamic simulations, we have chosen events with $N_{\text{part}} > 80$ for both the clustered and unclustered cases to understand the effects in the most-central collision scenario. It should be noted that such an event selection criterion in the Glauber model calculations with GLISSANDO [60] refers to almost similar centrality classes ($\approx$0–1 %) for both the clustered and unclustered cases. To study the effect of initial clustered structure on photon observables, we have considered a sufficiently large number of random events for both clustered and unclustered cases with the event selection criterion $N_{\text{part}} > 80$.

In Fig. 1, we show the N_{part} dependent behavior of clustered to unclustered ratio of the event-averaged (over 5×10^5 events) initial elliptic ($\langle \varepsilon_2^C \rangle / \langle \varepsilon_2^U \rangle$) and triangular eccentricities ($\langle \varepsilon_3^C \rangle / \langle \varepsilon_3^U \rangle$). We find that the ratio of elliptic eccentricities at various N_{part} are slightly less than 1, whereas, the the ratio for triangular eccentricities varies in the range 1.6–2.0 as a function of N_{part}. This clearly shows that the triangular anisotropies for the clustered case show more than 50% rise than the unclustered case for most central collisions. We have checked the initial eccentricities also with the TRENTO initial condition [61] and found a similar behavior of elliptic and triangular eccentricities with N_{part} for both the cluster and uncluster cases.

The event distribution of the α-clustered C + Au and the unclustered C + Au collisions in the $v_n - \varepsilon_n$ plane is shown in Fig. 2. The integrated v_n is obtained by integrating the differential thermal photon flow over the p_T range 0.5–6.0 GeV. The linear correlation (Pearson correlation) coefficient $C_n(\varepsilon_n, v_n)$ for both clustered and unclustered cases is shown for comparison. The correlation coefficient is defined as

$$C_n(\varepsilon_n, v_n) = \left\langle \frac{(\varepsilon_n - \langle \varepsilon_n \rangle)(v_n - \langle v_n \rangle)}{\sigma_{\varepsilon_n}\sigma_{v_n}} \right\rangle, \tag{2}$$

where the quantities without (with) angular bracket denote single event (event-averaged) values, σ_{ε_n} and σ_{v_n}, are the stan-

FIG. 3. The event-averaged thermal photon spectra from α-clustered C + Au and unclustered C + Au collisions at 200A GeV.
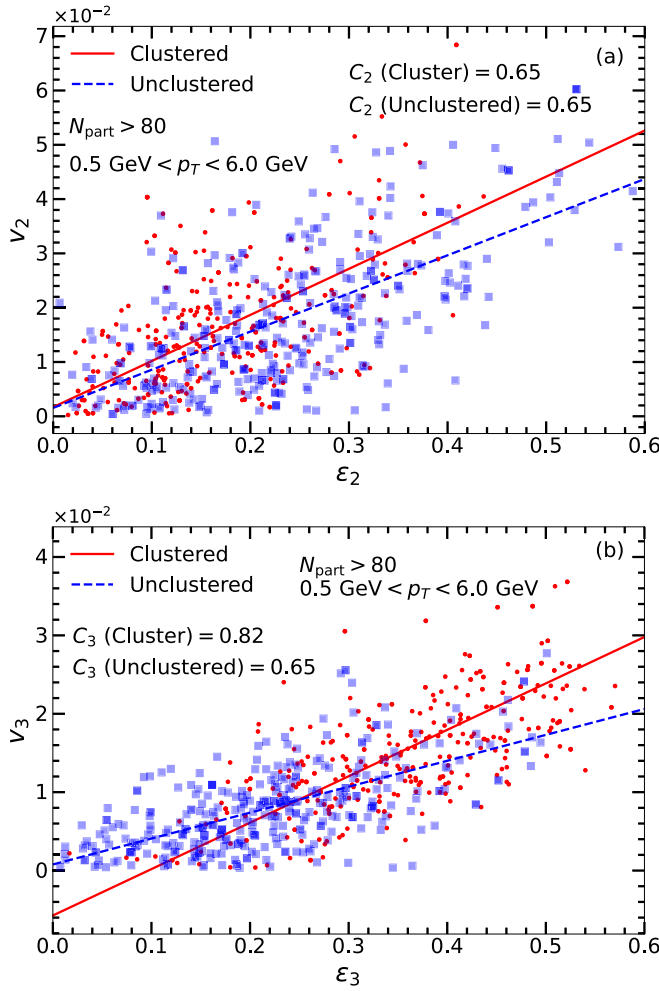
FIG. 2. The linear correlation between (a) v_2–ε_2 and (b) v_3–ε_3 for the α-clustered C + Au and the unclustered C + Au collisions at 200A GeV.

to each other which is consistent with the average initial elliptic eccentricities obtained for the respective cases. We see a slightly larger elliptic flow at $p_T \approx 2$ GeV for the unclustered case in comparison to the clustered case.

dard deviations of ε_n and v_n, respectively. To calculate the average of v_n, we use the integrated photon yield as weight, whereas, the total deposited energy on the transverse plane has been considered as the weight for calculating the average of initial state anisotropy. We see that the correlation coefficient between v_2 and ε_2 for the clustered and unclustered cases is similar (about 0.65). On the other hand, we see a stronger linear correlation (coefficient ≈ 0.82) in $v_3 - \varepsilon_3$ plane for the clustered carbon compared to the unclustered case (coefficient ≈ 0.65).

In Fig. 3, we show a comparison of the event-averaged thermal photon spectra from α-clustered and unclustered C + Au collisions. The spectra for both the cases are found to be close to each other. In the region $p_T > 4$ GeV, we observe a slight excess of photon production for the clustered case in comparison to the unclustered case which perhaps occurs due to the presence of initial hot spots in the clustered carbon case.

The event-averaged elliptic and triangular flow parameters of thermal photons as a function of p_T are presented in Figs. 4(a) and 4(b), respectively. The elliptic flow anisotropy for the clustered and unclustered cases is found to be close
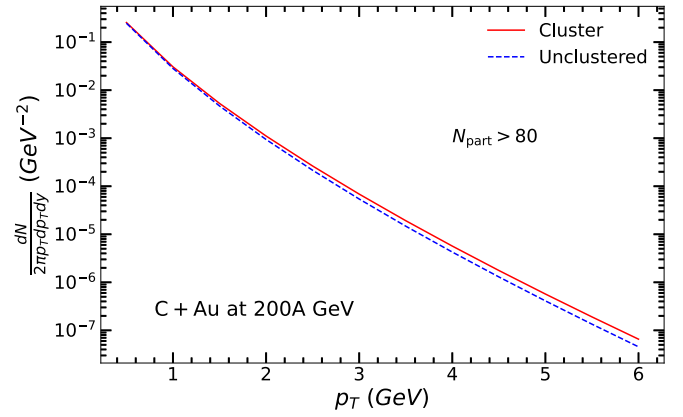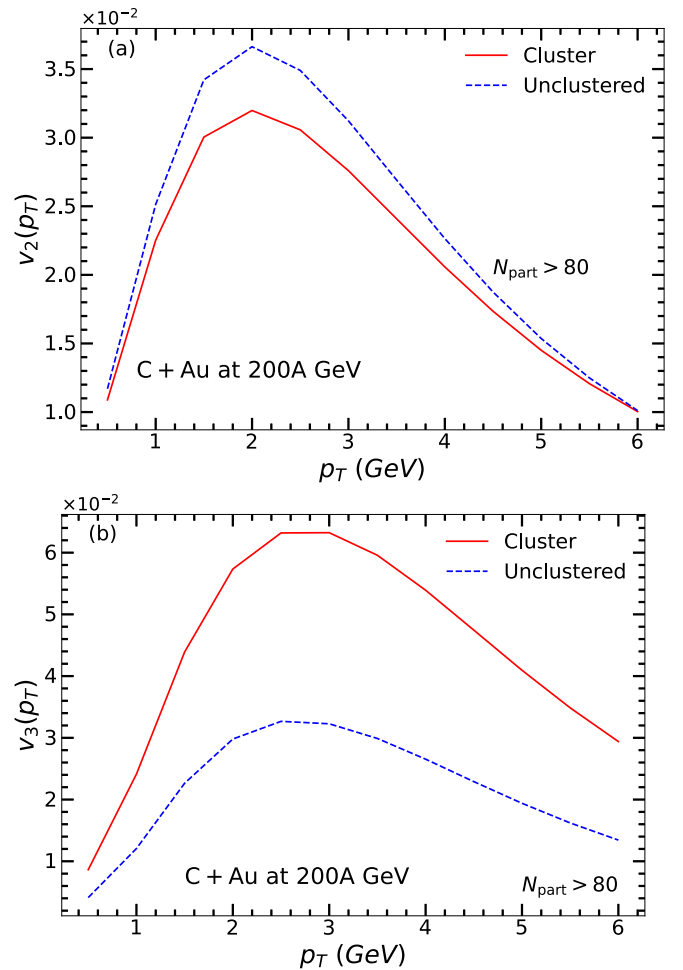

FIG. 4. (a) Elliptic and (b) triangular flow of thermal photons as a function of p_T from the α-clustered and unclustered C + Au collisions at 200A GeV.

However, v_3 for the clustered case is found to be twice as large as the same obtained for the unclustered case. It is to be noted that the orientation averaged triangular flow parameter for the clustered case is still significantly large and similar to the $v_3(p_T)$ obtained from most-central ($b \approx 0$ fm) collisions of α-clustered carbon with Au nucleus at an orientation angle $\theta = \pi/4$ (see Fig. 5(a) of Ref. [17]) considering smooth initial density distribution. Additionally, such large triangular flow anisotropy is also comparable to the direct photon v_3 data obtained for 20–40 % Au + Au collisions at the BNL Relativistic Heavy Ion Collider (RHIC). It is to be noted that a larger initial thermalization time τ_0 or a smaller freeze-out temperature (T_f) would further increase the value of thermal photon v_3 as discussed in Ref. [17]. These results clearly state that photon v_3 in relativistic nuclear collisions can efficiently reflect the initial state triangular anisotropy associated with the triangular α-cluster structure in carbon nucleus. It is also well known that a significant contribution of the prompt photons appears in the region $p_T > 3$ GeV [17] in the direct photon spectrum and it dominates over the thermal radiation in that p_T range. However, the prompt photons do not contribute directly to the anisotropic flow. These nonthermal photons only dilute the flow parameters in the larger p_T region by adding extra weight in the denominator of Eq. (5). One can still expect to get a large direct photon $v_3^{dir}(p_T)$ after including the nonthermal prompt contribution in the calculation [17].

In a recent study, it has been emphasized that the ratio of anisotropic flow coefficients (v_n/v_m) can minimize the uncertainties arising due to the nonthermal contributions [62] in the photon anisotropic flow calculation. The ratio is shown to be a potential observable to probe the thermal phase contribution in the direct photon anisotropic flow. Although the individual flow parameters (v_2, v_3) are found to underestimate the experimental v_n data of Au + Au collisions at RHIC, the photon v_2/v_3 of the same is found to be close to the PHENIX data in the p_T region 2–3.5 GeV, which is believed to be dominated by the thermal radiation. The ratio is also found to be sensitive to the initial conditions of the model calculation in different p_T regions compared to the individual flow parameters. The ratio of directed flow parameter with photon v_2 (or v_3) (along with the individual photon anisotropic flow parameters) provides additional information to constrain the initial parameters of the model calculation. We show the ratio of thermal photon v_2 to v_3 as a function of p_T in Fig. 5. The dashed line shows the ratio for the unclustered case which is found to be about 2 at $p_T \approx 1$ GeV and above $p_T > 3$ GeV, the ratio gets closer to 1. However, for the clustered case the ratio (solid line) is found to be smaller than 1 in the region $p_T > 1$ GeV, which in turn indicates a significantly larger thermal photon v_3 compared to the thermal photon v_2. We simultaneously show the ratio of thermal photon v_2 and v_3 from 0–20 % Au + Au collisions at RHIC (solid triangles) using the same hydrodynamical framework for comparison [62]. We find that the ratio for the central Au + Au collisions is closer to the result from unclustered C + Au collisions whereas the ratio from the clustered case is significantly smaller in the thermal (2–4 GeV) p_T range. Thus, experimental determination of photon v_2/v_3 ratio from C + Au collisions can be an impor-
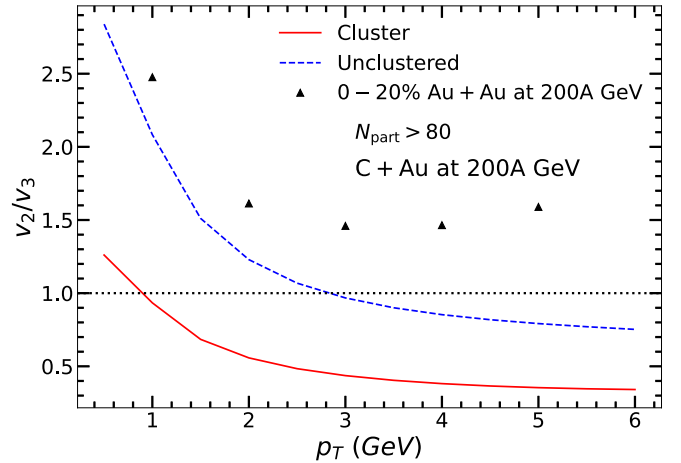

FIG. 5. The ratio of thermal photon v_2 and v_3 as function of p_T for the α-clustered and unclustered C + Au collisions at 200A GeV. The ratio of thermal photon v_2 to v_3 for 0–20 % Au + Au collisions at RHIC using the same hydrodynamic framework is shown for comparison [18].

tant observable to identify the clustered structure in carbon nucleus.

The directed flow of thermal photons from C + Au collisions is shown as a function of p_T in Fig. 6(a). The photon v_1 for both clustered and unclustered cases is found to be close to each other. This observation is consistent with the directed initial eccentricities obtained for the two cases. The linear correlation coefficient between p_T-integrated photon v_1 and ε_1 is found to be about -0.59 and -0.51 for the clustered and the unclustered cases, respectively (see Fig. 2 in the Supplemental Material [63]). We show the ratio of the directed flow of thermal photons with triangular flow in Fig. 6(b). The ratio is seen to be different in the region $p_T < 2$ GeV where the ratio for the clustered case is found to be larger than the unclustered case. In the region $p_T > 2$ GeV an opposite behavior is observed, however, the difference between the two is relatively smaller. The v_1/v_3 has been shown to be more sensitive to the hadronic phase unlike v_2/v_3 of photons [62]. Thus, the ratio of photon v_n can also be valuable to know about the freeze-out temperature of the evolving fireball.

Therefore, this study overall provides a qualitative understanding of thermal photon production and anisotropic flow from most-central α-clustered C + Au collisions at 200A GeV. It is to be noted that we have checked all the photon v_n results with the scalar product method [20,64] and also considering the lattice-based equation of state $s95p - v1$ [65] to see the sensitivity of our observations with the choice of the framework (see Appendix B). The qualitative nature of the results is found to remain the same irrespective of the method we chose. We also notice that the difference between the results on a quantitative scale is marginal only. A (3 + 1)-dimensional viscous hydrodynamical calculation is ideal to obtain more reliable results for C + Au collisions on a quantitative scale; however, according to Fig. 4 in Ref. [66], we cannot expect a significant change in the results for the most-central collision scenario.
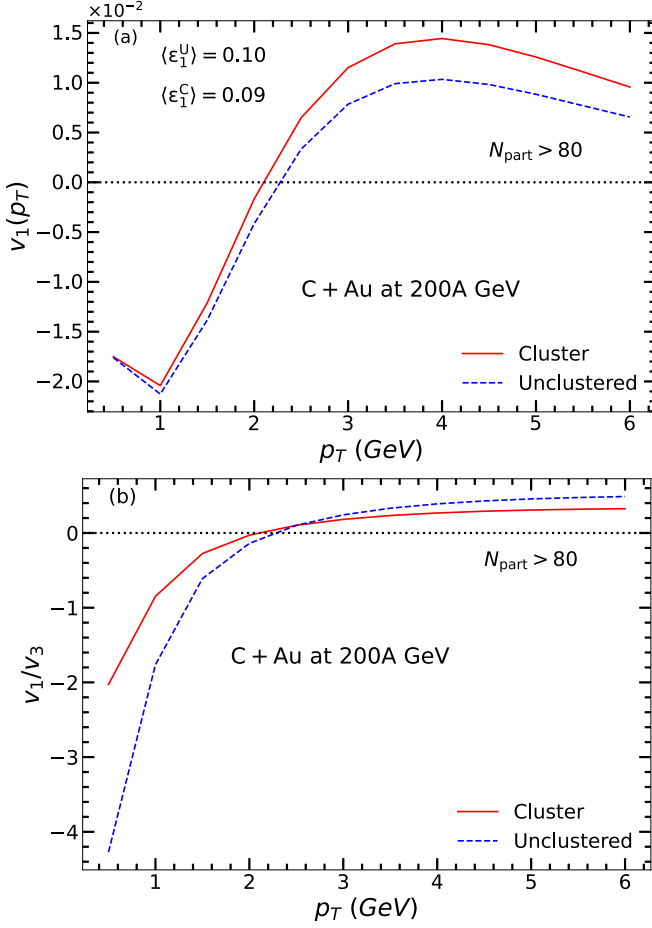
FIG. 6. (a) Directed flow of thermal photons and (b) its ratio with thermal photon v_3 for the α-clustered C + Au and the unclustered C + Au collisions at 200A GeV.

IV. SUMMARY

We calculate the production and anisotropic flow of thermal photons from most-central α-clustered C and Au collisions at 200A GeV using an event-by-event hydrodynamic framework and compare the results with those obtained from unclustered carbon and gold collisions. The slope of the thermal photon spectrum from the clustered carbon is found to be similar to the same obtained from the unclustered carbon. However, the clustered structure affects the initial triangular eccentricity as well as the triangular flow parameter of photons significantly compared to the unclustered carbon and gold collisions. Although we find a similar thermal photon v_2 for both clustered and unclustered carbon collisions, the thermal photon v_3 for the clustered case is found to be almost twice as large as the unclustered case.

In addition, we show that the ratio of photon anisotropic flow parameters (v_2/v_3) can be a useful observable to recognize the clustered structure in carbon nucleus. The v_2/v_3 ratio is found to be strongly sensitive to the α-cluster structure and is significantly suppressed compared to the unclustered case. We also show that the directed flow parameter of photons can be a potential observable along with the elliptic and triangular

flow parameters to constrain the initial state produced in heavy ion collision. We conclude that photon flow observables are potential probes to detect the α-cluster structure in carbon nucleus and experimental determination of the anisotropic flow parameters from C + Au collisions can be useful to study the initial state in relativistic heavy ion collisions.

APPENDIX A

In this Appendix, we discuss in detail the initial conditions of our model calculations and the method for calculating thermal photon flow observables.

1. Initial Conditions

We consider a triangle-shaped α-clustered carbon where the vertices of three α clusters reside at three corners of an equilateral triangle. The side length (l) of the triangle is 3.05 fm and the radius of each cluster (r_α) is 0.96 fm. The nuclear density distribution corresponding to each cluster follows:

$$f_i(\vec{r}) = A \exp\left(-\frac{3}{2}(\vec{r} - \vec{c}_i)^2/r_\alpha^2\right), \tag{A1}$$

where $\vec{c}_i$ denotes the position of the center of ith cluster in carbon. For the unclustered case, we take a two-parameter Woods-Saxon density profile in such a way that the root mean square radius of the unclustered carbon is similar to the clustered carbon (≈ 2.26 fm).

A two-component Monte Carlo Glauber (MCG) model framework is used to distribute the initial entropy density on the transverse plane for each event where entropy density at any transverse coordinate (x, y) is obtained using the following relation:

$$s(x, y) = K \sum_{i, j=1}^{N_{\mathrm{part}}, N_{\mathrm{coll}}} [\nu\, n_{\mathrm{coll}}(x_i, y_i) F_i(x, y)$$
$$+ (1 - \nu)\, n_{\mathrm{part}}(x_j, y_j)\, F_j(x, y)]. \tag{A2}$$

In the above equation, n_{coll} and n_{part} denote the number of binary collision and participant sources at the (x_i, y_i) and (x_j, y_j) positions, respectively. The values of nucleon-nucleon inelastic cross section (σ_{NN}), hardness factor (ν), and the normalization constant (K) are taken as 42 mb, 0.145 and 81 fm^{-1}, respectively. The function $F_i(x, y)$ [or $F_j(x, y)$] is a normalized Gaussian distribution centering about the ith

collision (or jth participant) source

$$F_{i,j}(x,y) = \frac{1}{2\pi\sigma^2} e^{-\frac{(x-x_{i,j})^2+(y-y_{i,j})^2}{2\sigma^2}}, \qquad (A3)$$

where the Gaussian smearing width (σ) of radius around each collision and participant source is considered as 0.4 fm [17].

The above set of the initial hydrodynamic parameters has been found to satisfactorily explain the charged hadron multiplicity and differential spectrum of π^0 at the midrapidity for most central (i.e., 0–5%) ^{3}He +Au collisions at 200A GeV at RHIC [67] (see Fig. 1 in the Supplemental Material [63]).

2. Participant Plane Method

The differential anisotropic flow coefficients [$v_n(p_T)$ for $n = 1, 2,$ and 3] for each event are obtained as

$$v_n(p_T) = \frac{\int_0^{2\pi} d\phi \cos[n(\phi-\psi_n)] \frac{dN}{p_T dp_T dy d\phi}}{\int_0^{2\pi} d\phi \frac{dN}{p_T dp_T dy d\phi}}, \qquad (A4)$$

where ϕ is the azimuthal angle of particle's momentum and ψ_n is the participant plane angle. We calculate the event-averaged final flow observables ($\langle v_n \rangle$, which we denote hereafter as v_n for simplicity) by using the following equation:

$$\langle v_n(p_T) \rangle = \frac{\sum_{i=1}^{N_{\text{events}}} \frac{dN^{(i)}}{d^2 p_T dy} v_n^{(i)}(p_T)}{\sum_{i=1}^{N_{\text{events}}} \frac{dN^{(i)}}{d^2 p_T dy}}. \qquad (A5)$$

In the above equations, the superscript 'i' corresponds to the ith event. The participant plane angle is determined by

$$\psi_n = \frac{1}{n} \arctan \frac{\int dx dy \, r^m \sin(n\Phi)\epsilon(x,y,\tau_0)}{\int dx dy \, r^m \cos(n\Phi)\epsilon(x,y,\tau_0)} + \pi/n. \quad (A6)$$

The initial-state eccentricities (ε_n, where $m = 3, 2,$ and 3 for $n = 1, 2,$ and 3, respectively [68,69]) for each event are obtained using the relation

$$\varepsilon_n = -\frac{\int dx dy \, r^m \cos[n(\Phi-\psi_n)]\epsilon(x,y,\tau_0)}{\int dx dy \, r^m \epsilon(x,y,\tau_0)}, \qquad (A7)$$

where Φ and r are spatial azimuthal angle and the radial distance, and ϵ is the energy density on the transverse plane.

APPENDIX B

Scalar Product Method

In this section, we calculate the photon flow observables from the most-central C + Au collisions at 200A GeV using the scalar product method [20,64]. Unlike the participant plane method, the scalar product method directly correlates the photon emission with the charged hadron event-plane angle. Therefore, it is more relatable to the experimental data. We use Monte Carlo Glauber initial conditions [Eq. (A2)] along with lattice-based equation state $s95p - v1$ [65] within
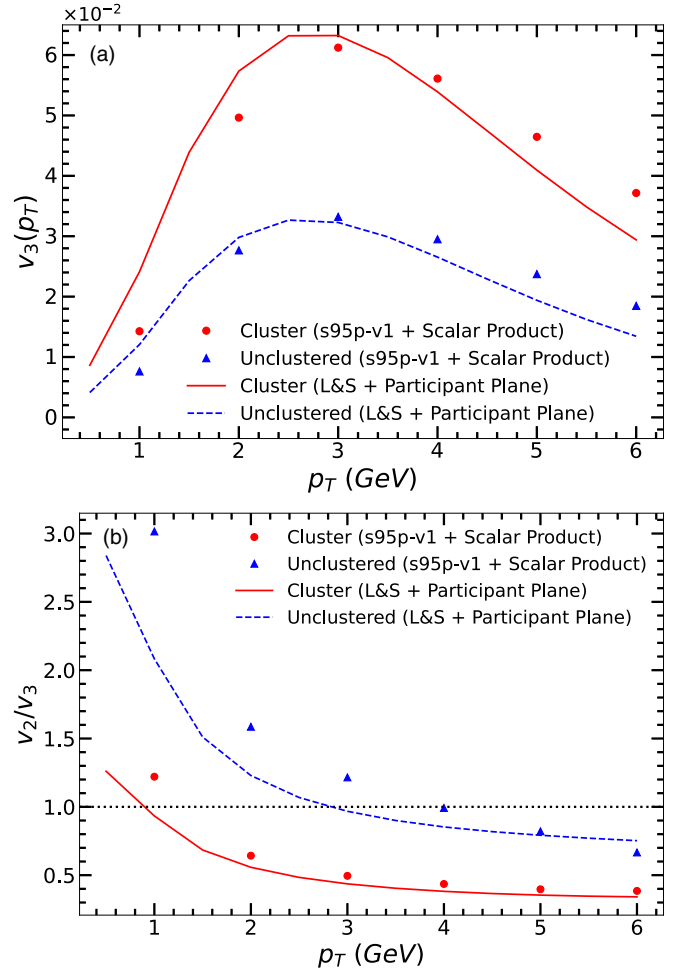

FIG. 7. The thermal photon (a) v_3 and (b) the ratio v_2/v_3 as a function of p_T using the scalar product method in the MUSIC ideal hydrodynamical framework for the α-clustered C + Au and the unclustered C + Au collisions at 200A GeV. The results have been compared with results presented earlier in Figs. 4(b) and 5.

the MUSIC ideal hydrodynamical framework [70] to calculate the spacetime evolution of the fireball. The other associated hydrodynamic parameters have been considered to be the same as presented in Sec. II.

In Fig. 7(a), we show the thermal photon v_3 as a function of p_T for the clustered and unclustered C + Au collisions using the scalar product method. The obtained results (represented by the solid symbols) are found to be very close to the earlier results using the participant plane angle method (represented by lines). Similar behavior has been found for the photon v_2/v_3 ratio as a function of p_T, as shown in Fig. 7(b). We conclude that the calculation method merely affects the qualitative difference between the photon flow observables from the clustered and unclustered C + Au collisions.

[1] D. K. Srivastava, J. Phys. G **35**, 104026 (2008).

[2] R. Chatterjee, E. S. Frodermann, U. W. Heinz, and D. K. Srivastava, Phys. Rev. Lett. **96**, 202302 (2006).

[3] C. Gale, Y. Hidaka, S. Jeon, S. Lin, J. F. Paquet, R. D. Pisarski, D. Satow, V. V. Skokov, and G. Vujanovic, Phys. Rev. Lett. **114**, 072301 (2015).

[4] R. Chatterjee, H. Holopainen, I. Helenius, T. Renk, and K. J. Eskola, Phys. Rev. C **88**, 034901 (2013).

[5] A. Monnai, Phys. Rev. C **90**, 021901(R) (2014).

[6] L. McLerran and B. Schenke, Nucl. Phys. A **929**, 71 (2014).

[7] G. Başar, D. E. Kharzeev, and V. Skokov, Phys. Rev. Lett. **109**, 202303 (2012).

[8] K. Tuchin, Phys. Rev. C **87**, 024912 (2013).

[9] B. G. Zakharov, Eur. Phys. J. C **76**, 609 (2016).

[10] R. Chatterjee, Pramana **95**, 15 (2021).

[11] G. Vujanovic, J. F. Paquet, G. S. Denicol, M. Luzum, B. Schenke, S. Jeon, and C. Gale, Nucl. Phys. A **932**, 230 (2014).

[12] F. M. Liu and S. X. Liu, Phys. Rev. C **89**, 034906 (2014).

[13] R. Chatterjee and D. K. Srivastava, Phys. Rev. C **79**, 021901(R) (2009).

[14] R. Chatterjee and D. K. Srivastava, Nucl. Phys. A **830**, 503c (2009).

[15] R. Chatterjee, H. Holopainen, T. Renk, and K. J. Eskola, Phys. Rev. C **85**, 064910 (2012).

[16] P. Dasgupta, R. Chatterjee, and D. K. Srivastava, Phys. Rev. C **95**, 064907 (2017).

[17] P. Dasgupta, G. L. Ma, R. Chatterjee, L. Yan, S. Zhang, and Y. G. Ma, Eur. Phys. J. A **57**, 134 (2021).

[18] A. Adare *et al.* (PHENIX Collaboration), Phys. Rev. C **94**, 064901 (2016).

[19] S. Acharya *et al.* (ALICE Collaboration), Phys. Lett. B **789**, 308 (2019).

[20] G. David, Rep. Prog. Phys. **83**, 046301 (2020).

[21] C. Shen, arXiv:1511.07708 [nucl-th].

[22] C. Gale, J. F. Paquet, B. Schenke, and C. Shen, Nucl. Phys. A **1005**, 121863 (2021).

[23] P. Dasgupta, R. Chatterjee, S. K. Singh, and J.-e. Alam, Phys. Rev. C **97**, 034902 (2018).

[24] I. Iatrakis, E. Kiritsis, C. Shen, and D. L. Yang, J. High Energy Phys. 04 (2017) 035.

[25] C. Aidala *et al.* (PHENIX Collaboration), Nat. Phys. **15**, 214 (2019).

[26] G. Aad *et al.* (ATLAS Collaboration), Phys. Rev. Lett. **116**, 172301 (2016).

[27] S. Chatrchyan *et al.* (CMS Collaboration), Phys. Lett. B **718**, 795 (2013).

[28] M. Rybczynski, M. Piotrowska, and W. Broniowski, Phys. Rev. C **97**, 034912 (2018).

[29] P. Bożek, W. Broniowski, E. R. Arriola and M. Rybczynski, Phys. Rev. C **90**, 064902 (2014).

[30] Y. A. Li, S. Zhang, and Y. G. Ma, Phys. Rev. C **102**, 054907 (2020).

[31] S. Zhang, Y. G. Ma, J. H. Chen, W. B. He, and C. Zhong, Phys. Rev. C **95**, 064904 (2017).

[32] J. He, W. B. He, Y. G. Ma, and S. Zhang, Phys. Rev. C **104**, 044902 (2021).

[33] G. Giacalone, J. Jia, and C. Zhang, Phys. Rev. Lett. **127**, 242301 (2021).

[34] J. Jia, Phys. Rev. C **105**, 014905 (2022).

[35] J. Jia, Phys. Rev. C **105**, 044905 (2022).

[36] H. j. Xu, H. Li, X. Wang, C. Shen, and F. Wang, Phys. Lett. B **819**, 136443 (2021).

[37] X. L. Zhao and G. L. Ma, Phys. Rev. C **106**, 034909 (2022).

[38] B. Bally, J. D. Brandenburg, G. Giacalone, U. Heinz, S. Huang, J. Jia, D. Lee, Y. J. Lee, W. Li, and C. Loizides *et al.*, arXiv:2209.11042.

[39] G. Gamow, *Constitution of Atomic Nuclei and Radioactivity* (Clarendon Press, Oxford, 1931), pp. viii and 114.

[40] C. W. Cook, W. A. Fowler, C. C. Lauritsen, and T. Lauritsen, Phys. Rev. **107**, 508 (1957).

[41] F. Hoyle, Astrophys. J. Suppl. **1**, 121 (1954).

[42] M. Freer, H. Horiuchi, Y. Kanada-En'yo, D. Lee, and U. G. Meißner, Rev. Mod. Phys. **90**, 035004 (2018).

[43] Y. Liu and Y. L. Ye, Nucl. Sci. Tech. **29**, 184 (2018).

[44] Z. Ren and B. Zhou, Front. Phys. **13**, 132110 (2018).

[45] Y. Kanada-En'yo, Prog. Theor. Phys. **117**, 655 (2007); **121**, 895 (2009).

[46] T. Neff and H. Feldmeier, Nucl. Phys. A **738**, 357 (2004).

[47] A. Tohsaki, H. Horiuchi, P. Schuck, and G. Ropke, Phys. Rev. Lett. **87**, 192501 (2001).

[48] B. Zhou, A. Tohsaki, H. Horiuchi, and Z. Ren, Phys. Rev. C **94**, 044319 (2016).

[49] T. A. Lähde, E. Epelbaum, H. Krebs, D. Lee, U. G. Meißner, and G. Rupak, Pramana **83**, 651 (2014).

[50] W. B. He, Y. G. Ma, X. G. Cao, X. Z. Cai, and G. Q. Zhang, Phys. Rev. Lett. **113**, 032506 (2014).

[51] W. B. He, Y. G. Ma, X. G. Cao, X. Z. Cai, and G. Q. Zhang, Phys. Rev. C **94**, 014301 (2016).

[52] B. S. Huang, Y. G. Ma, and W. B. He, Phys. Rev. C **95**, 034606 (2017).

[53] C. Z. Shi and Y. G. Ma, Nucl. Sci. Tech. **32**, 66 (2021).

[54] C. C. Guo, W. B. He, and Y. G. Ma, Chin. Phys. Lett. **34**, 092101 (2017).

[55] H. Holopainen, H. Niemi, and K. J. Eskola, Phys. Rev. C **83**, 034901 (2011).

[56] M. Laine and Y. Schroder, Phys. Rev. D **73**, 085009 (2006).

[57] P. B. Arnold, G. D. Moore, and L. G. Yaffe, J. High Energy Phys. 12 (2001) 009.

[58] J. Ghiglieri, J. Hong, A. Kurkela, E. Lu, G. D. Moore, and D. Teaney, J. High Energy Phys. 05 (2013) 010.

[59] S. Turbide, R. Rapp, and C. Gale, Phys. Rev. C **69**, 014903 (2004).

[60] W. Broniowski, M. Rybczynski, and P. Bozek, Comput. Phys. Commun. **180**, 69 (2009).

[61] J. S. Moreland, J. E. Bernhard, and S. A. Bass, Phys. Rev. C **92**, 011901(R) (2015).

[62] R. Chatterjee and P. Dasgupta, Phys. Rev. C **104**, 064907 (2021).

[63] See Supplemental Material at http://link.aps.org/supplemental/10.1103/PhysRevC.107.044908 for the differential spectrum of π^0 in 0–5 % central ^{3}He + Au collisions at 200A GeV (Fig. 1) and the linear correlation between $v_1 - \varepsilon_1$ for C+Au collisions at 200A GeV (Fig. 2).

[64] C. Shen, U. W. Heinz, J. F. Paquet, I. Kozlov, and C. Gale, Phys. Rev. C **91**, 024908 (2015).

[65] P. Huovinen and P. Petreczky, Nucl. Phys. A **837**, 26 (2010).

[66] C. Shen, J. F. Paquet, G. S. Denicol, S. Jeon, and C. Gale, Phys. Rev. C **95**, 014906 (2017).

[67] U. A. Acharya *et al.* (PHENIX Collaboration), Phys. Rev. C **105**, 064902 (2022).

[68] P. Dasgupta, R. Chatterjee, and D. K. Srivastava, J. Phys. G **47**, 085101 (2020).

[69] D. Teaney and L. Yan, Phys. Rev. C **83**, 064904 (2011).

[70] B. Schenke, S. Jeon, and C. Gale, Phys. Rev. C **82**, 014903 (2010).